

Hojamberdiev, Mirabbos; Kawashima, Kenta

Article

Exploring flux-grown transition metal oxynitride perovskites for photocatalytic water oxidation: A minireview

Energy Reports

Provided in Cooperation with:

Elsevier

Suggested Citation: Hojamberdiev, Mirabbos; Kawashima, Kenta (2020) : Exploring flux-grown transition metal oxynitride perovskites for photocatalytic water oxidation: A minireview, Energy Reports, ISSN 2352-4847, Elsevier, Amsterdam, Vol. 6, Iss. 4, pp. 13-24, <https://doi.org/10.1016/j.egyr.2019.09.021>

This Version is available at:

<https://hdl.handle.net/10419/244003>

Standard-Nutzungsbedingungen:

Die Dokumente auf EconStor dürfen zu eigenen wissenschaftlichen Zwecken und zum Privatgebrauch gespeichert und kopiert werden.

Sie dürfen die Dokumente nicht für öffentliche oder kommerzielle Zwecke vervielfältigen, öffentlich ausstellen, öffentlich zugänglich machen, vertreiben oder anderweitig nutzen.

Sofern die Verfasser die Dokumente unter Open-Content-Lizenzen (insbesondere CC-Lizenzen) zur Verfügung gestellt haben sollten, gelten abweichend von diesen Nutzungsbedingungen die in der dort genannten Lizenz gewährten Nutzungsrechte.

Terms of use:

Documents in EconStor may be saved and copied for your personal and scholarly purposes.

You are not to copy documents for public or commercial purposes, to exhibit the documents publicly, to make them publicly available on the internet, or to distribute or otherwise use the documents in public.

If the documents have been made available under an Open Content Licence (especially Creative Commons Licences), you may exercise further usage rights as specified in the indicated licence.



<https://creativecommons.org/licenses/by-nc-nd/4.0/>



Exploring flux-grown transition metal oxynitride perovskites for photocatalytic water oxidation: A minireview

Mirabbos Hojaberdiiev ^{a,b,*}, Kenta Kawashima ^c

^a Institut für Werkstoffwissenschaften und -technologien, Technische Universität Berlin, Hardenbergstraße 40, 10623 Berlin, Germany

^b Uzbekistan-Japan Innovation Center of Youth, University Street 2, 100095 Tashkent, Uzbekistan

^c Department of Chemistry, The University of Texas at Austin, Austin, TX 78712, United States

ARTICLE INFO

Article history:

Available online 17 September 2019

Keywords:

Oxynitride
Perovskite
Photocatalyst
Solar water splitting
Flux growth
Doping
Solid solution

ABSTRACT

Transition metal oxynitride perovskites $[AB(O,N)_3]$ are an emerging class of inorganic materials with superior light harvesting ability (narrow band-gap energy) and moderate photostability. They can be utilized as visible-light-active photocatalysts for efficient solar water splitting. The photocatalytic activity of transition metal oxynitride perovskites has been significantly improved by changing the synthesis approach, reducing the defect density that acts as a recombination center for photogenerated charge carriers, increasing the conductivity, and engineering their band structures, namely the conduction and valence band positions, through an A/B -site doping/substitution. In this minireview, we briefly overview our recent advances on enhancing the photocatalytic activity of selected transition metal oxynitride perovskites (i.e., LaTiO_2N , BaTaO_2N , and BaNbO_2N) and related works. Additionally, the challenges and future perspectives of these materials are discussed.

1. Introduction

1.1. Background

The semiconductor-based photocatalytic water splitting using solar energy is regarded as one of the promising technologies to produce hydrogen as a clean and renewable fuel (Zou et al., 2001; Lee, 2005; Maeda et al., 2006; Maeda and Domen, 2010; Maeda, 2011; Osterloh, 2013). In the early stage of this research area, metal oxide-based semiconducting materials were extensively studied. However, most oxides possess a relatively large band-gap ($E_g > 3.0$ eV), hindering the efficient utilization of solar energy. Consequently, this led to the shift of a research interest from wide-band-gap materials to narrow-band-gap materials that can absorb visible light efficiently. Currently, a number of research groups in the world are intensively working on enhancement of solar-to-hydrogen (STH) conversion efficiency of those visible-light-active photocatalysts. In general, overall water splitting into hydrogen and oxygen is mainly limited by the slow kinetics of the oxygen evolution reaction (Liu et al., 2015). This is because the oxygen evolution reaction is accomplished by a 4-electron transfer ($4\text{OH}^- \rightarrow \text{O}_2 + 2\text{H}_2\text{O} + 4\text{e}^-$), whereas the hydrogen

evolution reaction is achieved by a 2-electron reduction ($2\text{H}^+ + 2\text{e}^- \rightarrow \text{H}_2$). Therefore, it is necessary to further improve the oxygen evolution activity of visible-light-active photocatalysts.

1.2. Transition metal oxynitride perovskites for photocatalytic water oxidation

The d^0 -type transition metal (Ti, Nb, Ta, or W) oxynitride perovskites, $AB(O,N)_3$ (A - larger alkali, alkaline earth, or rare earth metal cations; B - smaller transition metal cations) (Fig. 1A), having the ability to photocatalytically oxidize water have been studied (Momma and Izumi, 2011). As shown in Fig. 1B, transition metal oxynitride perovskites are able to absorb visible light because of the N 2p orbital with a higher potential energy compared to O 2p orbital (Maeda and Domen, 2011, 2007). To improve the photocatalytic water splitting activity of transition metal oxynitride perovskites, the following approaches have been applied: (i) flux method (also known as molten salt method) to increase the crystallinity, (ii) novel oxide precursor to reduce the defects and to enlarge the specific surface area, and (iii) A/B -site doping/substitution (including some sort of solid solutions) to prolong and increase the lifetime and mobility of photogenerated electrons and holes and/or to engineer the conduction band (CB) and valence band (VB) positions. Particularly, this minireview turns the spotlight on our recent progress on improving the photocatalytic water splitting (especially about photocatalytic water oxidation) of a few members of transition metal oxynitride family, such as LaTiO_2N , BaTaO_2N , and BaNbO_2N , and other

DOI of original article: <https://doi.org/10.1016/j.egyr.2019.08.067>.

* Corresponding author at: Institut für Werkstoffwissenschaften und -technologien, Technische Universität Berlin, Hardenbergstraße 40, 10623 Berlin, Germany.

E-mail address: hmirabbos@ceramics.tu-berlin.de (M. Hojaberdiiev).

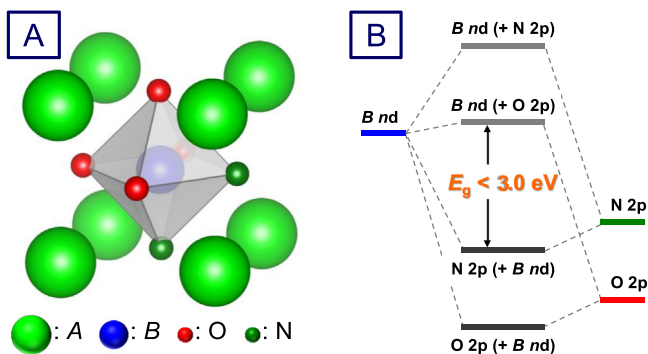


Fig. 1. (A) Crystal structure and (B) band structure of a typical d^0 -type transition metal oxynitride perovskite $[AB(O,N)_3]$.
Source: The band structure was reprinted from Ref. Maeda and Domen (2007) with permission.
© 2007 American Chemical Society.

related works. The challenges and future perspectives of these materials for designing the high-performance photocatalysts for water splitting are discussed briefly.

2. LaTiO₂N

Perovskite-type lanthanum titanium oxynitride (LaTiO₂N) has a narrow band-gap of ~ 2.1 eV [theoretical STH conversion efficiency: $\sim 16\%$ (Chen et al., 2013)] and an *n*-type semiconducting nature, and its structure belongs to *Imma* space group (Kasahara et al., 2002, 2003; Zhang et al., 2012; Yashima et al., 2010). LaTiO₂N has been widely studied as one of the promising photocatalysts for solar water splitting. It can harvest photons from the visible region of solar spectrum and can separately produce hydrogen and oxygen with suitable sacrificial reagents (e.g., methanol for hydrogen evolution and AgNO₃ for oxygen evolution) and cocatalysts (e.g., Pt for hydrogen evolution and IrO₂ or CoO_x for oxygen evolution) (Kasahara et al., 2002, 2003; Zhang et al., 2012) and also exhibits interesting optical and dielectric properties (Moriga et al., 2007; Tessier and Marchand, 2003).

2.1. Effect of flux-assisted nitridation process

It is known that LaTiO₂N can be synthesized by a general synthetic approach — nitridation. In the nitridation process, the La₂Ti₂O₇ precursor synthesized by a soft-chemistry method (Maegli et al., 2012a,b), a polymerized complex (PC) method (Kasahara et al., 2002), or a sol-gel method (Kasahara et al., 2003) is treated by thermal ammonolysis (nitridation) under an NH₃ flow. Due to the long nitridation process, solid-state transformation of crystal structure from oxide to oxynitride, and low crystallinity of oxide precursors, LaTiO₂N is formed with a low crystallinity and a large amount of defects acting as a recombination center for photogenerated charge carriers, reducing the photocatalytic efficiency. In order to improve the crystallinity and to reduce the defect density, we have previously introduced a flux method for the synthesis of La₂Ti₂O₇ crystals (route A in Fig. 2) and an NH₃-assisted flux method for the direct synthesis of LaTiO₂N crystals (route C in Fig. 2). As a result, the photocatalytic performance of LaTiO₂N for water oxidation was significantly improved (Kasahara et al., 2003; Maegli et al., 2012b; Wagata et al., 2014; Hojamberdiev et al., 2015a). At elevated temperature, the fluxes can form a completely ionized non-aqueous high-temperature solution where crystals grow freely and gain their idiomorphic shapes. Also, in the absence of temperature gradient, the flux method allows crystal growth with minimized crystal defects (e.g., dislocations, vacancies, etc.) and mechanical and thermal strains. Therefore, the flux method is advantageous for improving the crystallinity, tailoring the morphology

and size, and surface modification of transition metal oxynitride perovskites (Kawashima et al., 2015; Abeysinghe and Skrabalak, 2018). Particularly, Maegli et al. (2013) studied the flux-assisted nitridation processes (routes B and D in Fig. 2) for the synthesis of LaTiO₂N. To further evaluate effects of the flux-assisted nitridation processes of LaTiO₂N, LaTiO₂N synthesized by route A was compared with LaTiO₂N synthesized by route C (Kawashima et al., 2015). Note that the routes B, C, and D were almost same because LaTiO₂N was formed via two-step reactions in route C (Kawashima et al., 2015):

1st step:



2nd step:



As shown in Fig. 2, although there is no significant difference in their nitrogen contents (*y* values in Fig. 2) and specific surface areas ($10.6 \text{ m}^2 \text{ g}^{-1}$ for A; $8.6 \text{ m}^2 \text{ g}^{-1}$ for C) (Kawashima et al., 2015; Tessier et al., 2005; Tessier, 2018), LaTiO₂N from route C demonstrated a higher oxygen evolution rate than LaTiO₂N from route A. This is because the flux-assisted nitridation process improved the crystallinity and modified the surface of LaTiO₂N (Kawashima et al., 2015; Maegli et al., 2013). However, once the CoO_x cocatalyst was loaded on LaTiO₂N, all the LaTiO₂N samples exhibited similar oxygen evolution rates due to different dispersion of CoO_x cocatalyst nanoparticles. Compared to LaTiO₂N synthesized by a flux-assisted nitridation (route C in Fig. 2), LaTiO₂N synthesized by a normal nitridation (route A in Fig. 2) might contain more dangling bonds that can act as nucleation centers for CoO_x nanoparticles (Maegli et al., 2013) on the surface of LaTiO₂N. Consequently, the CoO_x nanoparticles have higher dispersion on the surface of LaTiO₂N from route A, giving rise to the oxygen evolution rate. In contrast, CoO_x nanoparticles have lower dispersion on the surface of LaTiO₂N from route C, leading to the lower oxygen evolution rate. Considering the above discussions in this section, the flux-assisted nitridation is essential to enhance the photocatalytic activity of LaTiO₂N itself through improving the crystallinity and reducing the defect density.

2.2. Effect of oxide precursors (La₂Ti₂O₇ vs. La₂TiO₅)

The use of La₂TiO₅ (a lanthanum-rich oxide precursor) instead of La₂Ti₂O₇ (a stoichiometric oxide precursor) for the synthesis of LaTiO₂N is another possibility to lower the number of defects (e.g., reduced Ti species) (Kawashima et al., 2014). However, this defect generation suppression has not been clarified, which needs to be investigated further in the future. Furthermore, LaTiO₂N synthesized from La₂TiO₅ has a significantly higher

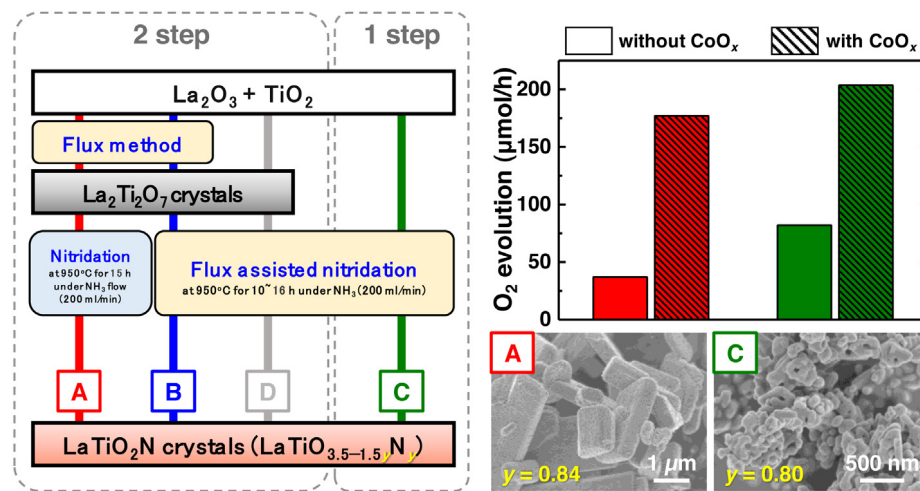


Fig. 2. Four synthesis routes of LaTiO_2N crystal structures (left) and scanning electron microscope (SEM) images and photocatalytic oxygen evolution rates for first 2 h of LaTiO_2N crystal structures (right). Photocatalytic reaction conditions: photocatalyst – 0.10 g; pH buffer (La_2O_3) – 0.20 g; reaction solution (10 mM AgNO_3 aqueous solution) – 200 mL; light source – 300 W Xe lamp ($\lambda > 420$ nm cutoff filter).

Source: SEM images and photocatalytic oxygen evolution data were adapted from Ref. Kawashima et al. (2015) with permission.
 © 2014 American Chemical Society.

specific surface area than LaTiO_2N synthesized from $\text{La}_2\text{Ti}_2\text{O}_7$ (Zhang et al., 2012; Kawashima et al., 2014). Recently, Xiong et al. (2017) reported the photocatalytic oxygen evolution performance of LaTiO_2N synthesized from $\text{La}_2\text{Ti}_2\text{O}_7$ and La_2TiO_5 with/without Co_3O_4 cocatalyst (Fig. 3). According to their study, pristine LaTiO_2N synthesized from La_2TiO_5 had a lower [Fermi level (E_F)] – [VB maximum (E_{VBM})]_{surface}, resulting in the lowest water oxidation performance despite the fact that this sample had a lower defect density. They also found that annealing in Ar gas could increase the $E_F - E_{\text{VBM_surface}}$ of LaTiO_2N synthesized from La_2TiO_5 , giving rise to its photocatalytic water oxidation performance (Xiong et al., 2017) which is higher than that of LaTiO_2N from $\text{La}_2\text{Ti}_2\text{O}_7$. Hence, both the use of La-rich oxide precursor to lower the defect density in LaTiO_2N and annealing in Ar gas to improve the crystallinity of LaTiO_2N surface without inducing the formation of reduced titanium species are important to maximize the $E_F - E_{\text{VBM_surface}}$ for enhancing the photocatalytic water oxidation performance (Xiong et al., 2017; Seo et al., 2018).

2.3. Effects of A-site substitution and B-site doping

The A-site substitution is another promising approach to control the O/N ratio in the final oxynitride product, affecting the energy position of valence band. For instance, Logvinovich et al. (2007) and Cheviré et al. (2006) found that the nitrogen content can be decreased and the band-gap energy might be increased when La^{3+} is substituted for $\text{Ca}^{2+}/\text{Sr}^{2+}$ in LaTiO_2N (Fig. 4A) because $\text{Ca}^{2+}/\text{Sr}^{2+}$ content increase probably decreases the total cationic charge in LaTiO_2N , resulting in its lower total anionic charge which attributed to increased O/N ratios [i.e., $\text{La}^{3+}{}_{1-x}\text{A}^{2+}{}_x\text{Ti}^{4+}\text{O}^{2-}{}_{2+x}\text{N}^{3-}{}_{1-x}$ ($\text{A} = \text{Ca}, \text{Sr}; x = 0, 0.3, 0.5, 0.7, 1.0$ for $\text{Ca}; x = 0, 0.25, 0.5, 0.75, 0.90, 1$ for Sr)]. Maegli et al. (2012a) also reported the Ca^{2+} -backfilled LaTiO_2N with the low Ca content ($x = 0, 0.05, 0.10, 0.20, 0.30$) which did not change the band-gap energy. Additionally, the 5% Ca^{2+} -backfilled LaTiO_2N showed the highest oxygen evolution activity due to its low defect concentration (Ti^{3+}) and improved crystallinity (enlarged crystallite size) (Maegli et al., 2012b). Furthermore, according to the other report about Ca^{2+} -substituted LaTiO_2N (Kawahara et al., 2002), the $\text{Ca}_{0.25}\text{La}_{0.75}\text{Ti}_{0.25}\text{N}_{0.75}$ also exhibited a higher oxygen evolution activity than pristine LaTiO_2N . More recently, Wu et al. (2017) investigated the $\text{La}_{1-x}\text{Ca}_x\text{TiO}_{2+x}\text{N}_{1-x}$ ($x = 0, 0.3, 0.5, 0.7, 0.9, 1.0$)

again and discovered that the $\text{Ca}_{0.3}\text{La}_{0.7}\text{TiO}_{2.7}\text{N}_{0.3}$ unexpectedly exhibited the quite narrow band-gap of 1.63 eV and the high oxygen evolution performance [$\sim 66.96 \mu\text{mol h}^{-1}$] under visible light ($\lambda \geq 420$ nm) owing to a substantial reduction of surface Ti^{3+} species and a removal of A-site cation segregation by the Ca incorporation. In addition, it was revealed that the Ca incorporation can enhance the photogenerated charge mobility of LaTiO_2N (Wu et al., 2017). However, in band-gap, the trend published in a 2002 paper does not match with that in a 2017 paper (see $x = 0.5$ and 0.7), as seen in Fig. 4A. This mismatch may mainly come from the difference in the synthetic approaches (further investigation is necessary). The B-site doping is another important approach for enhancing the photocatalytic activity. Recently, the tungsten doping on titanium site in LaTiO_2N significantly prolonged the lifetime of photogenerated charge carriers and enhanced the photocatalytic activity for water oxidation (Fig. 4B) (Kawashima et al., 2016a), which is also supported by the related studies on tungsten doping in BaTaO_2N (Maeda et al., 2013a) and Ta_3N_5 (Grigorescu et al., 2015). From the first-principles density functional theory (DFT) calculations, a slight broadening of the valence and conduction bands was observed in tungsten-doped LaTiO_2N , which may improve the electron/hole conductivity owing to the reduction of the effective mass of electrons (Kawashima et al., 2016a). Accordingly, the combination of A-site substitution and B-site doping can further improve the photocatalytic activity of LaTiO_2N for water oxidation, and this possibility is currently under investigation.

3. BaTaO_2N

As a member of alkaline-earth-based transition-metal oxynitride perovskites, BaTaO_2N crystallizes in cubic crystal structure with the space group of $Pm\bar{3}m$ (no. 221) (Marchand et al., 1986; Pors et al., 1988). BaTaO_2N is one of the promising candidates for solar water oxidation because of its narrow band-gap ($E_g = 1.8$ eV), visible light absorption up to 680 nm, and nontoxicity (Hojamberdiev et al., 2015b). Moreover, the conduction band minimum (CBM) and valence band maximum (VBM) of BaTaO_2N were estimated to be at -0.4 and 1.5 V versus the normal hydrogen electrode at $\text{pH} = 0$, respectively, theoretically allowing water splitting in the absence of an external bias voltage (Wang et al., 2016). Comparing three different crystal structures

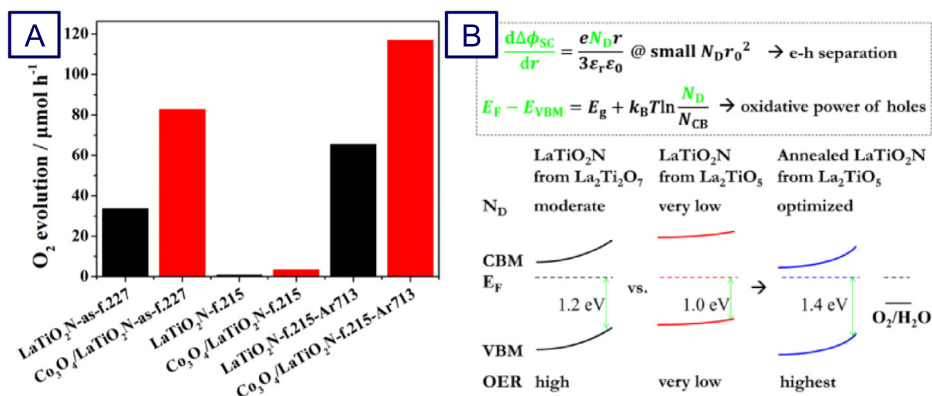


Fig. 3. (A) Comparison of photocatalytic oxygen evolution rates (first 0.5 h) and (B) the donor density and the difference between E_F and E_{VBM} of LaTiO₂N crystal structures. Photocatalytic reaction conditions: photocatalyst - 0.10 g; pH buffer (La₂O₃) - 0.10 g; reaction solution (10 mM AgNO₃ aqueous solution) - 100 mL; light source - 300 W Xe lamp ($\lambda > 420$ nm cutoff filter).

Source: Reprinted from Ref. Xiong et al. (2017) with permission.

© 2017 WILEY-VCH Verlag GmbH & Co. KGaA.

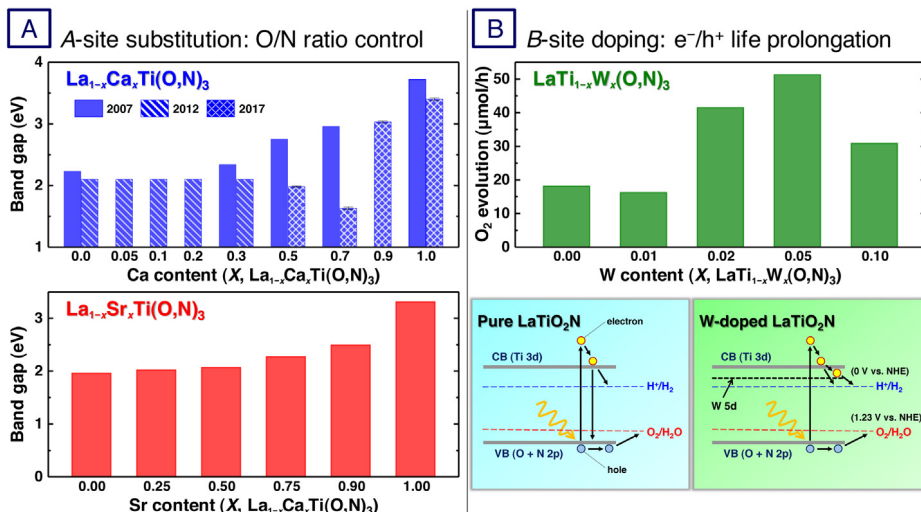


Fig. 4. (A) Band-gap energy dependence on Ca/Sr content in LaTiO₂N and (B) photocatalytic oxygen evolution dependence of W content in LaTiO₂N. Photocatalytic reaction conditions: photocatalyst - 0.10 g; pH buffer (La₂O₃) - 0.20 g; reaction solution (10 mM AgNO₃ aqueous solution) - 200 mL; light source - 300 W Xe lamp ($\lambda > 420$ nm cutoff filter). Reprinted/adapted from Refs. Logvinovich et al. (2007), Cheviré et al. (2006), Maegli et al. (2012a,b) and Wu et al. (2017) with permission. Copyright 2007, Elsevier; Copyright 2006, WILEY-VCH Verlag GmbH & Co. KGaA; and Copyright 2012, The Royal Society of Chemistry. Reprinted from Ref. Kawashima et al. (2016a) with permission. Copyright 2016, The Royal Society of Chemistry.

of BaTaO₂N, Bettine et al. (2017) found that the electronic and optical properties are strongly related with the TaO₄N₂ octahedral configurations, whereas the band-gap is influenced by the internal electric fields which creates an asymmetry in the Ta–N bond lengths, and the minimum band-gaps of the P4mm, I4/mmm, and Pmma structures were predicted to be 1.83, 1.59, and 1.49 eV, respectively.

As a member of the promising 600 nm-class oxynitride photocatalysts family, BaTaO₂N can potentially generate a photocurrent of about 18 mA cm⁻² under AM 1.5G light based on the assumption of incident photon-to-current conversion efficiency (IPCE) value of 100% at < 660 nm (Ueda et al., 2015). Incidentally, the theoretical STH conversion efficiency of BaTaO₂N is about 24% (Chen et al., 2013). The IPCE value of BaTaO₂N fabricated by electrophoretic deposition with surface modification was estimated to be about 10% at 1.2 V versus the reversible hydrogen electrode (RHE) at 600 nm, which is the highest among the photoanode materials that can harvest light beyond 600 nm (Higashi et al., 2013). The BaTaO₂N showed STH conversion efficiency of 0.7% at 1.0 V_{RHE}, and the BaTaO₂N modified with a Co cocatalyst generated a photocurrent of 4.2 mA cm⁻² at 1.2 V_{RHE} (Ueda et al., 2015).

Recently, the Ir/Co/BaTaO₂N exhibited a photocurrent and a half-cell STH energy conversion efficiency at 0.7 V_{RHE} of 0.26 mA cm⁻² and 0.14%, respectively (Higashi et al., 2017), which are three times higher than those obtained previously for Co/BaTaO₂N. In addition to its solar water splitting activity, BaTaO₂N can also exhibit an extremely high and temperature-independent dielectric constant both in polycrystalline and in thin film forms, providing the possibility for technological applications in electronics industries (Kim et al., 2004) and has a potential to be used in CO₂ reduction (Hafez et al., 2016).

3.1. Effects of synthesis methods and morphological control

The photocatalytic activity can be enhanced through the synthesis of materials with large surface area, high dispersion, high crystallinity, low defect density, defined morphology, and specifically exposed facets, allowing to reduce the number of recombination sites and to increase photocatalytically active sites. Particularly, one- and two-dimensional crystals can significantly enhance the photocatalytic activity by increasing the active sites

on the surface and decreasing the travel distance of photogenerated electrons and holes. However, the morphology control and nanostructure fabrication of BaTaO₂N have been challenging. BaTaO₂N was routinely synthesized by a two-step method: (i) the synthesis of a corresponding oxide precursor and (ii) its high-temperature nitridation under an NH₃ atmosphere, which leads to the self-decomposition during the high-temperature nitridation. The anion vacancies act as recombination centers for photogenerated charge carriers, reducing the photocatalytic water splitting activity (Pors et al., 1988; Kim et al., 2004; Maeda and Domen, 2007). Several approaches have been developed to synthesize phase-pure BaTaO₂N. Cordes et al. (2018) synthesized BaTaO₂N crystals with the size of 1–10 μm by the ammonothermal method at 900 K and maximum pressures of up to 300 MPa in a custom-built autoclave using Ba and Ta metals, and NaN₃ and NaOH which were used as mineralizers. Recently, Niu et al. (2018) succeeded the synthesis of phase-pure BaTaO₂N with a homogeneous particle size distribution and slightly off-stoichiometric composition under NH₃-free atmosphere using BaCO₃ and TaN as starting materials and nitrogen source. Sun et al. (2015) developed a facile method to directly synthesize nearly single-phase powders of BaTaO₂N by heat treatment of BaCO₃ and Ta₃N₅ (nitrogen source) in flowing N₂. Under AM 1.5G, the BaTaO₂N thin film fabricated on a conductive substrate and deposited with a CoPi layer exhibited a photocurrent of ~0.75 mA cm⁻² at 1.23 V_{RHE} and produced oxygen for 5 h with a Faradaic efficiency of > 90% without significant deactivation (Wang et al., 2016). Setsuda et al. (2017) synthesized BaTaO₂N crystals at low temperature using NaNH₂ with different NaNH₂/Ta molar ratios, and the highest photocatalytic hydrogen and oxygen evolution was observed for the BaTaO₂N synthesized with the NaNH₂/Ta molar ratio of 3 because of its higher crystallinity and lower defect density associated with reduced Ta³⁺ species.

Flux method is one of the single-crystal growth techniques and applied to grow high-quality crystals with different morphologies, sizes, and surface features in supersaturated nonaqueous high-temperature solution (Bugaris and zur Loyer, 2012; Boltersdorf et al., 2015). Particularly, crystals with clear crystal habits (e.g., cubes, plates, etc.) grown by a flux method can be advantageous to develop a photocatalytic system with a monolayer of single crystals (1–10 μm) (Moriya et al., 2013). Previously, we applied the flux growth method to synthesize La_{1-x}Sr_xFe_{1-y}Ti_yO₃ (Hojamberdiev et al., 2017a), CdTiO₃, Cd₂Nb₂O₇, Cd₂Ta₂O₇ (Hojamberdiev et al., 2016a), Ba₅Nb_{4-x}Ta_xO₁₅ (Hojamberdiev et al., 2016b), ZnIn₂S₄ (Hojamberdiev et al., 2018), LaTaON₂, PrTaON₂ (Hojamberdiev et al., 2017b), BaNb_{0.5}Ta_{0.5}O₂N (Kawashima et al., 2018a), and N-doped ZnTiO₃ (Wagata et al., 2019) crystals with less defect density, increased surface area, improved particle dispersion and/or high crystallinity. Dong et al. (2017) synthesized BaTaO₂N by employing Ba-rich LiBa₄Ta₃O₁₂ prepared by a flux method and exhibited much higher hydrogen evolution activity both in half reaction and in Z-scheme overall water splitting due to the decreased defect density and surface area enhancement. Previously, we explored the effects of various fluxes (KCl, KI, KF, MgCl₂, CaCl₂, SrCl₂, BaCl₂, K₂SO₄, K₂MoO₄, and K₂CO₃), holding temperature (700–950 °C), reaction time (0–10 h), and solute concentration (1–50 mol %) on the formation of BaTaO₂N crystals using BaCO₃ and Ta₂O₅ under NH₃ flow. It was found that cubic BaTaO₂N crystals with an average size of 125 nm could be grown by an NH₃-assisted flux growth method using KCl flux at 950 °C for 10 h and exhibited higher photocatalytic activity for hydrogen and oxygen evolution (Fig. 5A–C) (Hojamberdiev et al., 2015b). The flux growth of cubic BaTaO₂N crystals was proposed to proceed through the decomposition of BaCO₃, dissolution of BaO and Ta₂O₅ in the KCl flux, formation and dissolution of BaTa₂O₆ and Ba₅Ta₄O₁₅ intermediates, and formation of cubic BaTaO₂N crystals (Fig. 5D).

We also studied the effects of altered morphology and size on visible-light-induced water oxidation activity and photoelectrochemical performance of BaTaO₂N crystal structures. In this study, BaTaO₂N was synthesized by nitridation of the Ba₅Ta₄O₁₅ precursor crystals, grown by flux method using BaCl₂, KCl, RbCl, CsCl, KCl+BaCl₂, and K₂SO₄ at different solute concentrations, with and without KCl flux. The BaTaO₂N crystal structures obtained by nitridation without KCl flux showed higher surface areas than their counterparts prepared by nitridation with KCl flux because of the formation of porous networks (Fig. 6A). The BaTaO₂N crystal structures synthesized by nitridation without KCl flux exhibited high anodic photocurrents compared with the BaTaO₂N samples obtained by nitridation with KCl flux due to the high number of dangling bonds that acted as nucleation centers for highly dispersed CoO_x nanoparticles. The BaTaO₂N samples with smaller particle size exhibited low photoelectrochemical performance and photocatalytic oxygen evolution activities compared to their counterparts with larger particle sizes because of the high number of interparticle boundaries and surface degradation (Fig. 6B–C) (Hojamberdiev et al., 2019).

It is known that the cocatalyst–photocatalyst interface and dispersion of cocatalyst on photocatalyst surface play an important role in particulate-based photocatalysis. Recently, Okamoto et al. (2019) increased the O₂ evolution rate 3-fold by annealing under an N₂ flow after loading the Co species on the surface of BaTaO₂N crystals compared to that prepared by annealing under an NH₃ flow. Subsequent annealing under an H₂ atmosphere significantly exposed the BaTaO₂N surface as a result of the aggregation of CoO_x particles and further enhanced the photocatalytic O₂ evolution by a factor of two, yielding an apparent quantum efficiency of 0.55% at 420 nm. This was achieved due to the formation of an intimate contact enabling an efficient charge transfer at the interface.

3.2. Effects of A-/B-site partial substitution and combination with other semiconductors

Doping is one of the effective strategies to tune the electronic structure, band-gap, light absorption, and crystal size and to control the separation and migration of charge carriers (Kudo and Miseki, 2009). For instance, an increase in the content of calcium partially substituted for tantalum in BaTaO₂N led to the enlargement of band-gap and the decrement of defect levels and nitrogen content. A significant color variation suggests that calcium was successfully substituted and the visible light absorption was altered in BaTaO₂N (Fig. 7A). The photocatalytic activity for water oxidation and photocatalytic self-decomposition of BaTaO₂N were significantly improved and suppressed by calcium modification, respectively. Nearly 3-fold enhancement in oxygen evolution was achieved in BaCa_{0.10}Ta_{0.90}O_{2.27}N_{0.73} compared to pure BaTaO₂N, and an apparent quantum efficiency approached as high as about 2.1% at 420 ± 20 nm, which is the highest value reported for BaTaO₂N to date (Wei et al., 2018). To control the donor density in the bulk for improving the performance of photoelectrochemical water splitting on porous BaTaO₂N photoanodes under visible light, various dopants (Mo⁶⁺, W⁶⁺, Zr⁴⁺, and Ti⁴⁺) for Ta⁵⁺ were examined. The partial substitution of Ta⁵⁺ in BaTaO₂N by Mo⁶⁺ was found to increase the donor density and photoelectrochemical performance effectively (Higashi et al., 2015). Moon et al. (2016) developed a novel synthetic strategy, which accomplishes cation intercalation with concomitant anion substitution, for developing new oxynitrides phases. The partial replacement of (Ta,N) in BaTaO₂N by (Mg,O) or (Li/Na,O) modified the electronic structure. The compositional variation (BaLi_{0.2}Ta_{0.8}O_{2.8}N_{0.2}, BaNa_{0.2}Ta_{0.8}O_{2.8}N_{0.2}, and BaMg_{0.2}Ta_{0.8}O_{2.6}N_{0.4}) could control the lattice iconicity, optical band-gap, and color, which are important in potential application in photocatalysis (Fig. 7B).

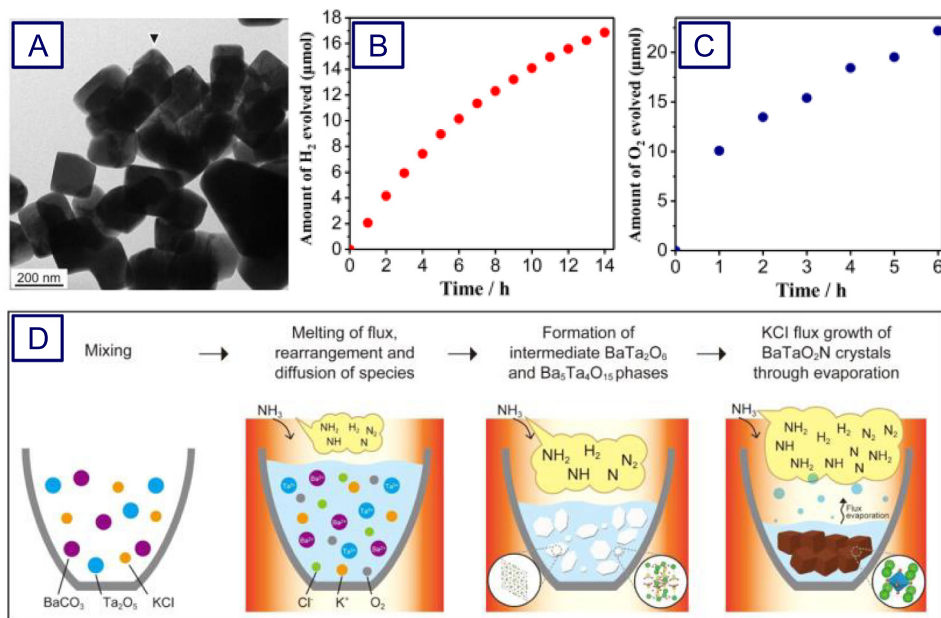


Fig. 5. (A) Transmission electron microscope (TEM) image, reaction time courses of (B) hydrogen and (C) oxygen evolution over cubic BaTaO₂N crystals under visible light irradiation. (D) Possible growth mechanisms of cubic BaTaO₂N crystals.
Source: Reprinted from Ref. Hojamberdiev et al. (2015b) with permission.
© 2015 American Chemical Society.

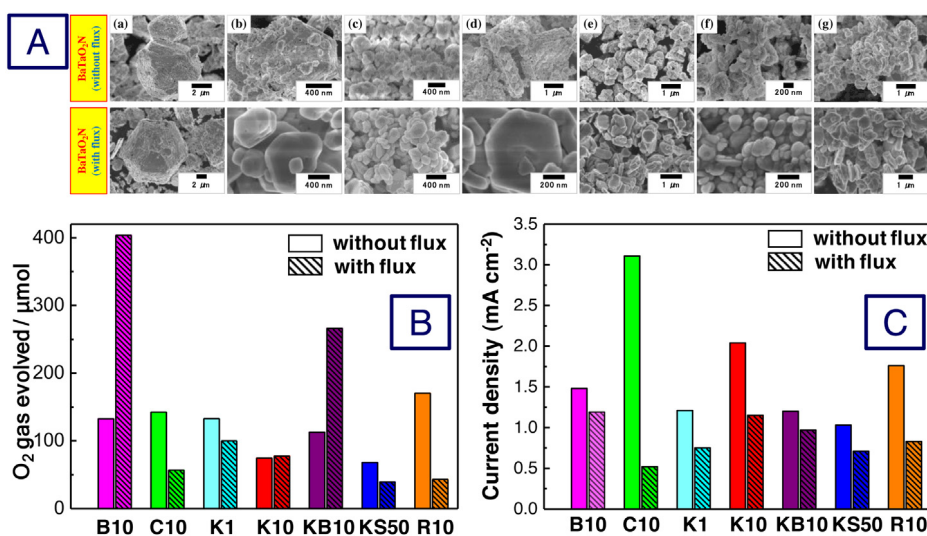


Fig. 6. (A) SEM images and (B) comparison of the amount of photocatalytically evolved oxygen (first 3 h) and (C) photocurrent density at 1.2 V_{RHE} of BaTaO₂N crystal structures obtained by nitridation of Ba₅Ta₄O₁₅ crystals, grown using BaCl₂ and 10 mol% sol. conc. (a, pink), CsCl and 10 mol% sol. conc. (b, green), KCl and 1 mol% sol. conc. (c, light blue), KCl and 10 mol% sol. conc. (d, red), KCl+BaCl₂ and 10 mol% sol. conc. (e, purple), K₂SO₄ and 50 mol% sol. conc. (f, blue), and RbCl and 10 mol% sol. conc. (g, orange), at 950 °C for 20 h with and without KCl flux. (For interpretation of the references to color in this figure legend, the reader is referred to the web version of this article.)

Source: Reprinted from Ref. Hojamberdiev et al. (2019) with permission.
© 2019 The Royal Society of Chemistry.

Another promising way of extending the light absorption to longer wavelength and improving the photocatalytic hydrogen and oxygen evolution is to combine BaTaO₂N with other semiconductor. Higashi et al. (2009) achieved overall water splitting into H₂ and O₂ under visible light by combining Pt–BaTaO₂N and Pt–WO₃ in the presence of IO₃⁻/I⁻ as a shuttle redox mediator. Maeda and Domen (2012) demonstrated that BaZrO₃–BaTaO₂N solid solutions (0 ≤ Zr/Ta ≤ 0.1) having a single-phase perovskite structure and band-gaps of 1.7–1.8 eV can reduce and oxidize water, giving H₂ and O₂, respectively, under visible light

irradiation above 660 nm. As shown in Fig. 8A, the BaWO_xNy–BaTaO₂N (W/Ta = 0.05) exhibited much higher water oxidation activity than the pristine BaTaO₂N and BaZrO₃–BaTaO₂N solid solution despite an increased density of d electrons originating from pentavalent W species (Maeda et al., 2013b). The cubic solid solution of (BaTaO₂N)_{1-x}(SrWO₂N)_x ($x = 0.01$) also exhibited higher photocatalytic activity for oxygen evolution in comparison to the pristine BaTaO₂N (Fig. 8B) (Hibino et al., 2017). In the BaWO_xNy–BaTaO₂N and (BaTaO₂N)_{1-x}(SrWO₂N)_x, the introduced W⁵⁺ species formed a donor level just below the conduction band, strengthening the n-type semiconducting character of

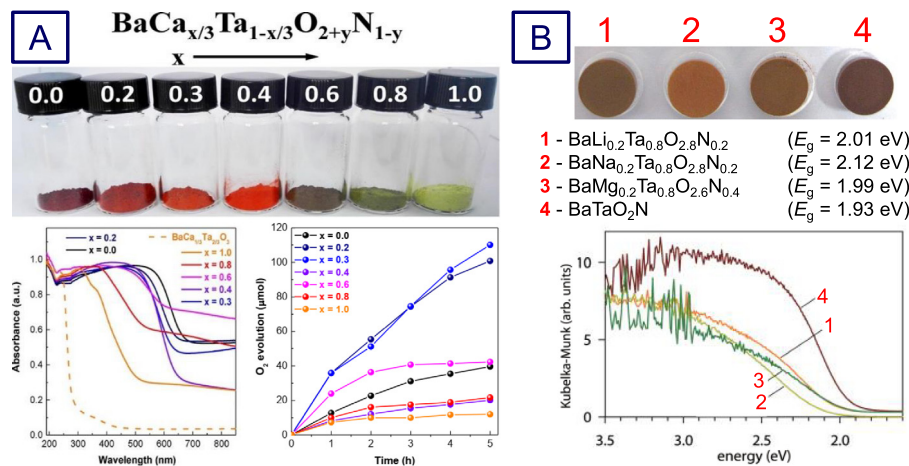


Fig. 7. (A) Digital photographs, ultraviolet-visible (UV-Vis) absorption spectra and photocatalytic oxygen evolution of $\text{BaCa}_{x/3}\text{Ta}_{1-x/3}\text{O}_{2+y}\text{N}_{1-y}$ ($0 \leq x, y \leq 1$) and (B) digital photographs and UV-Vis absorption spectra of $\text{BaLi}_{0.2}\text{Ta}_{0.8}\text{O}_{2.8}\text{N}_{0.2}$, $\text{BaNa}_{0.2}\text{Ta}_{0.8}\text{O}_{2.8}\text{N}_{0.2}$, $\text{BaMg}_{0.2}\text{Ta}_{0.8}\text{O}_{2.6}\text{N}_{0.4}$, and BaTaO_2N . Reprinted from Refs. Kudo and Miseki (2009) and Higashi et al. (2015) with permission. Copyright 2018, Elsevier and 2016, The Royal Society of Chemistry.

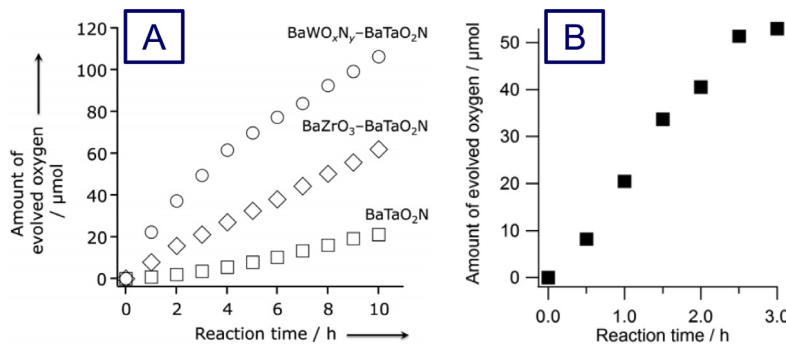


Fig. 8. (A) Time courses of the oxygen evolution on BaTaO_2N , $\text{BaTaO}_2\text{N}-\text{BaZrO}_3$, and $\text{BaWO}_x\text{N}_y-\text{BaTaO}_2\text{N}$ ($\text{W}/\text{Ta} = 0.005$) under visible light irradiation. Photocatalytic reaction conditions: photocatalyst - 0.10 g (1.5 wt% IrO₂-loaded); pH buffer (La_2O_3) - 0.10 g; reaction solution (10 mM AgNO₃ aqueous solution) - 100 mL; light source - 300 W Xe lamp ($\lambda > 420$ nm cutoff filter). (B) Time course of the oxygen evolution on $(\text{BaTaO}_2\text{N})_{0.99}(\text{SrWO}_3)_{0.01}$ under visible light irradiation. Photocatalytic reaction conditions: photocatalyst - 0.10 g (0.5 wt% IrO₂-loaded); pH buffer (La_2O_3) - 0.10 g; reaction solution (10 mM AgNO₃ aqueous solution) - 150 mL; light source - 300 W Xe lamp ($\lambda > 420$ nm cutoff filter). Reprinted from Refs. Maeda and Domen (2012) and Maeda et al. (2013b) with permission. Copyright 2013, WILEY-VCH Verlag GmbH & Co. and Copyright 2017, The Royal Society of Chemistry.

BaTaO₂N, leading to upward band bending. The photogenerated holes in the valence band could easily migrate to the surface according to the upward band-bending, enhancing the water oxidation activity.

4. BaNbO₂N

Barium niobium oxynitride perovskite, which crystallizes in cubic system with the space group of $Pm\bar{3}m$, is active for water oxidation under visible light irradiation up to $\lambda = 730$ nm ($E_g = 1.7$ eV) (Siritanaratkul et al., 2011), which indicates that its theoretical STH conversion efficiency is approximately 27% (Chen et al., 2013). Formerly, BaNbO₂N was also studied as a capacitor and superconductor (Cohen and Riess, 1994; Strukova et al., 1997).

4.1. Effects of oxide precursors

The synthesis routes of BaNbO₂N crystals are compiled in Fig. 9. BaNbO₂N is generally synthesized by high-temperature nitridation of a typical oxide precursor - Ba₅Nb₄O₁₅. Using the flux growth method, Yamada et al. (2018) controlled the size of Ba₅Nb₄O₁₅ crystals in the range of 0.2–50 μm and used them as sacrificial templates to obtain porous BaNbO₂N secondary particles that exhibited a distinctive photocatalytic activity for oxygen

evolution with rates between 14.1 and 113.9 μmol h⁻¹, depending on the precursor size and nitriding time. Since Ba₅Nb₄O₁₅ is Ba-rich, it requires the removal of excess Ba species after nitridation by acid treatment, leading to poor crystallinity and a large number of surface defects, which negatively affect the photocatalytic performance. Hisatomi et al. (2013) found that the addition of BaCO₃ to the Ba₅Nb₄O₁₅ precursor could improve the crystallinity and uniformity of BaNbO₂N, leading to higher photocatalytic oxygen evolution activity, and the apparent quantum efficiency of the oxygen evolution reaction was measured to be 0.04% at 640 ± 30 nm. Seo et al. (2016) achieved an appreciable improvement in photocurrent (0.85 mA cm⁻² at 1.23 V_{RHE}) during photoelectrochemical water oxidation using BaNbO₂N synthesized by nitridation of cubic-perovskite BaNbO₃, which is crystallographically similar to BaNbO₂N. Using BaNbO₃ as an oxide precursor enhanced the surface and bulk crystallinity of BaNbO₂N compared to the use of Ba₅Nb₄O₁₅ because the identical cubic-perovskite-type structural transition during nitridation minimized the formation of surface anion defects.

In addition, niobium is more prone to reduction under reducing atmosphere compared to tantalum, promoting the formation of a large number of defects associated with reduced niobium species in addition to anionic defects that act as recombination center for photogenerated charge carriers (Hojamberdiev et al., 2016c). Interestingly, higher barium/niobium ratios could effectively suppress the reduction of Nb⁵⁺ because the generation of

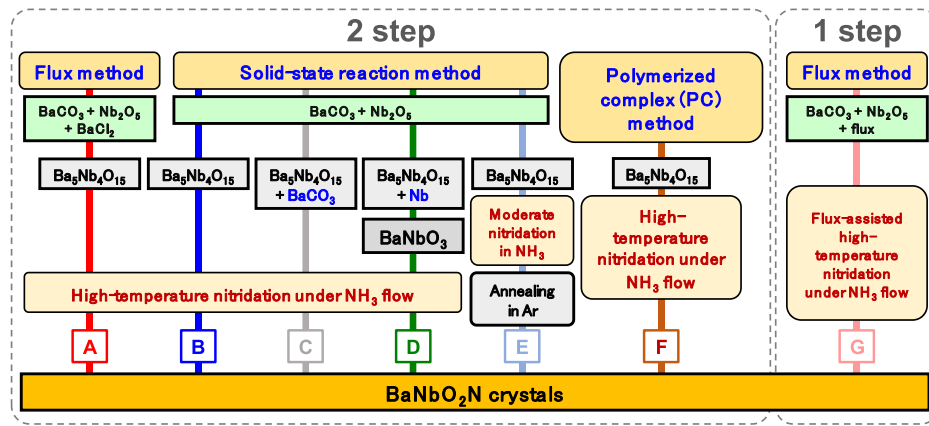


Fig. 9. Reported synthesis routes for BaNbO_2N crystals.

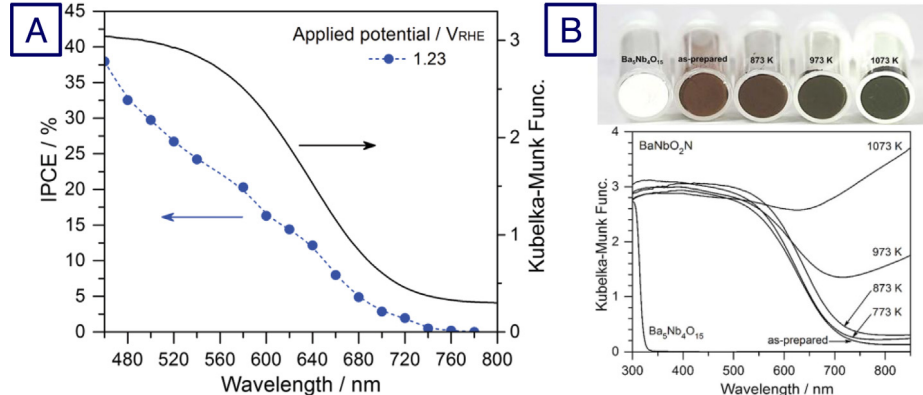


Fig. 10. (A) Wavelength dependence of the IPCE for a $\text{Co}(\text{OH})_x\text{-FeO}_x/\text{BaNbO}_2\text{N}$ photoanode measured at an applied potential of $1.23 \text{ V}_{\text{RHE}}$ over the wavelength range of $460\text{--}780 \text{ nm}$. (B) Digital photographs and UV-Vis diffuse reflectance spectra of the $\text{Ba}_5\text{Nb}_4\text{O}_{15}$ oxide precursor and the resulting BaNbO_2N series following nitridation at 1123 K for 15 h and subsequent annealing in an Ar atmosphere at $773, 873, 973$, and 1073 K for 1 h . Reprinted from Refs. Seo et al. (2016, 2019) with permission. Copyright 2014 and 2018, WILEY-VCH Verlag GmbH & Co.

$\text{Nb}(\text{O},\text{N})$ from the direct reaction of Nb_2O_5 with NH_3 could be inhibited. In this regard, the use of oxide precursor prepared by a PC method was more preferable because the niobium source could be homogeneously mixed with the barium source. As a result, BaNbO_2N prepared by a PC method exhibited 30% higher photocatalytic activity than that prepared by a solid-state reaction method due to the lower densities of reduced niobium and anion defects (Hisatomi et al., 2014). The synthesis route, consisting of moderate nitridation in NH_3 flow and subsequent annealing in inert Ar flow, enhanced the crystallinity and lowered the defect density of the BaNbO_2N surface without inducing the reduction of the Nb species (Seo et al., 2019). As a result, a particulate BaNbO_2N photoanode exhibited a photocurrent of 5.2 mA cm^{-2} at $1.23 \text{ V}_{\text{RHE}}$ under simulated solar irradiation, which is the highest yet reported for an oxynitride responsive at wavelengths above 600 nm (Seo et al., 2018). As shown in Fig. 10A, the IPCE of $\text{Co}(\text{OH})_x\text{-FeO}_x/\text{BaNbO}_2\text{N}$ photoanode at applied potential of $1.23 \text{ V}_{\text{RHE}}$ reached 1.9% at 720 nm and 38% at 460 nm . In the range of $600\text{--}680 \text{ nm}$, the IPCE values were still above 5% , suggesting that BaNbO_2N can harvest more visible light. The onset wavelength for photocurrent is in good agreement with the light absorption edge (Seo et al., 2018). As shown in Fig. 10, the white color of $\text{Ba}_5\text{Nb}_4\text{O}_{15}$ powders changed to brown for the as-prepared BaNbO_2N after moderate nitridation and darkened and become completely black with increasing the annealing temperature in Ar flow, suggesting the increase in the defect density (Seo et al., 2019). This is consistent with the UV-Vis diffuse reflectance spectra in Fig. 10B.

4.2. Effects of flux growth and B-site substitution

It is known that the morphological factors, such as crystal habit, dimension, crystallinity, deficiency, specific surface area, porosity, and so forth, play an important role in photocatalytic activity. Flux method enables us to control the morphology of crystals if suitable flux is selected by taking into account the material fundamental parameters (e.g., ionic radius, melting point, chemical bonding iconicity, Dietzel's parameter, acidity, basicity, etc.) (Oishi et al., 1984; Kawashima et al., 2018b; Teshima et al., 2017). Kodera et al. (2016) studied the influence of alkali-halide flux treatment with LiCl , NaCl , KCl , RbCl , CsCl , KF , KBr , or KI on morphology of the BaNbO_2N particles synthesized by a solid-state reaction method. When NaCl or CsCl were used as the flux, highly crystalline cubic particles were obtained, while using KCl , KBr , KI , or RbCl resulted in the formation of the truncated octahedral shapes. It was found that the kind of cation in the flux affected the morphology of BaNbO_2N rather than the kind of anion in the flux. Previously, we studied the cross-substitution effect of tantalum ions on the physical and visible-light-driven photocatalytic water oxidation activity of BaNbO_2N crystals grown directly by an NH_3 -assisted flux method (Hojamberdiev et al., 2016c). Clearly, an increase in the tantalum amount could reduce an average crystal size and change the crystal morphology from idiomorphic 3D to plate-like 2D (Fig. 11A). As shown in Fig. 11B, the intensity of background absorption in the UV-Vis diffuse reflectance spectra was gradually decreased due to the lesser amount of the reduced niobium species and anion deficiency. The oxygen evolution rate

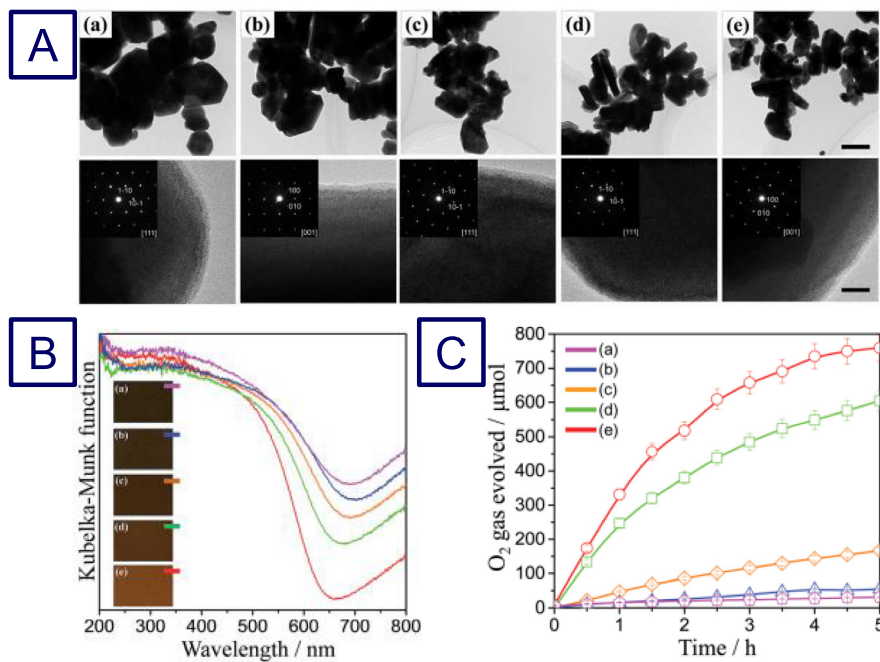


Fig. 11. (A) TEM and high-resolution TEM images and selected area diffraction patterns, (B) UV-Vis diffuse reflectance spectra, and (C) time courses of the oxygen evolution of (a) BaNbO₂N, (b) BaNb_{0.75}Ta_{0.25}O₂N, (c) BaNb_{0.50}Ta_{0.50}O₂N, (d) BaNb_{0.25}Ta_{0.75}O₂N, and (e) BaTaO₂N crystals. Photocatalytic reaction conditions: photocatalyst - 0.10 g (CoO_x-loaded); pH buffer (La₂O₃) - 0.20 g; reaction solution (10 mM AgNO₃ aqueous solution) - 300 mL; light source - 300 W Xe lamp ($\lambda > 420$ nm cutoff filter).

Source: Reprinted from Ref. Hojamberdiev et al. (2016c) with permission.
© 2016 The Royal Society of Chemistry.

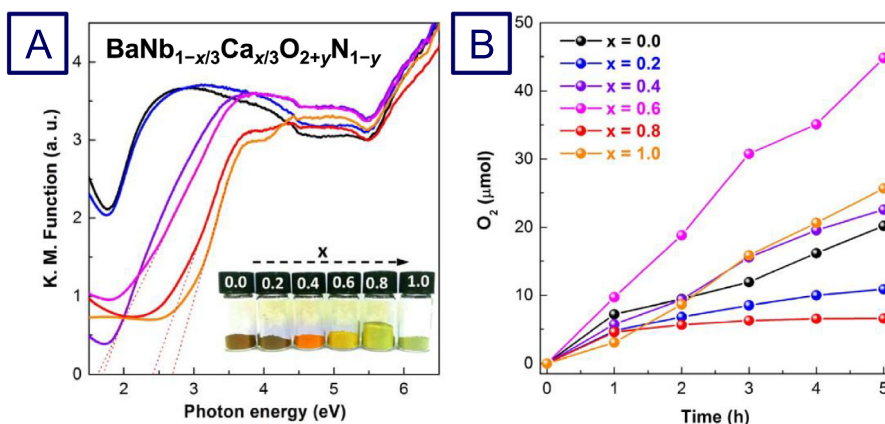


Fig. 12. (A) Kubelka-Munk transformation of diffuse reflectance data and digital photographs, and (B) photocatalytic oxygen evolution of BaNb_{1-x/3}Ca_{x/3}O_{2+y}N_{1-y} (0 \leq x, y \leq 1).

Source: Reprinted from Ref. Wei et al. (2019) with permission.
© 2019 WILEY-VCH Verlag GmbH & Co.

was increased monotonically and reached the maximum value of 331.1 μmol in the first 1 h for BaTaO₂N crystals loaded with a CoO_x (2 wt% Co) cocatalyst (Fig. 11C) owing to the shift of the valence band to a more positive side and the lowered densities of mid-gap states (Vequizo et al., 2018).

Quite recently, Wei et al. investigated the effect of Ca substitution into the B-site of BaNbO₂N on its properties and photocatalytic water oxidation (Wei et al., 2019). As shown in Fig. 12A, the band gap of the resultant compounds was enlarged along with Ca substitution level in BaNbO₂N. As comparison with pristine BaNbO₂N, more than 2-fold enhancement in photocatalytic oxygen evolution was accomplished by BaNb_{0.8}Ca_{0.2}O_{2+y}N_{1-y}

(x = 0.6). This improvement might be derived from the suppression of Nb⁴⁺ species in their structures and enhanced surface hydrophilicity after Ca modification (Fig. 12B) (Wei et al., 2019).

5. Conclusion and future perspective

In this minireview, various effective approaches, including flux method to increase crystallinity, novel oxide precursor to reduce the defects and to enlarge the specific surface area, and A/B-site doping/substitution to prolong the lifetime of photogenerated electrons and holes and/or to engineer the conduction band and valence band positions, to achieving higher water oxidation performance of selected transition metal oxynitride perovskites were presented. In recent years, significant efforts were made to improve the efficiency and stability of water oxidation over selected

transition metal oxynitride perovskites (i.e., LaTiO_2N , BaTaO_2N , and BaNbO_2N). As an example, a photocurrent of 5.2 mA cm^{-2} at $1.23 \text{ V}_{\text{RHE}}$ under simulated solar irradiation was recently achieved for the BaNbO_2N photoanode, which is the highest yet reported for an oxynitride responsive at wavelengths above 600 nm (Seo et al., 2018). Despite a remarkable progress in this research area, the quantum efficiency of these perovskites is still low and needs to be further improved to achieve better STH energy conversion efficiency. There are some promising approaches to enhance the water oxidation activity: (i) partial co-substitution of A-site and B-site cations in these parent perovskites by foreign cations that could change their band edge positions and electronic properties; (ii) creation of solid solutions of these perovskites with other semiconductors having an identical crystal structure and appropriate band edge positions; (iii) development of new methods [e.g., flux-coating method (Kawashima et al., 2017b)] and post-treatment to synthesize these perovskites with low defect density and to improve the surface properties as well as photostabilities, and (iv) exploration of new members of these perovskites family [e.g., MgTaO_2N (Kubo et al., 2017), AW(O,N)_3 ($A = \text{Sr, La, Pr, Nd, Eu}$) (Kawashima et al., 2016b, 2019), RHfO_2N ($R = \text{La, Nd, Sm}$) (Black et al., 2018), etc.] which were experimentally and computationally screened to be suitable photocatalysts for water oxidation (Montoya et al., 2015). These approaches are expected to improve STH energy conversion efficiency. In addition to the performance problems most of the transition metal oxynitride perovskites are still not able to exhibit the high photostability during the long-term oxygen evolution testing and tend to show rapid performance degradation due to the formation of their oxide counterparts on their surfaces (Kawashima et al., 2017b). Their photo-oxidation can also be confirmed by the significant amount of nitrogen gas evolution during the test (Kawashima et al., 2017a). According to the very recent DFT study on SrTaO_2N surface layers (Ouhbi and Aschner, 2019), it was confirmed that photo-oxidized surface layer leads tensile-strain-induced localization of excess charge at the surface which results in a stronger binding of oxygen evolution reaction intermediates (i.e., $^*\text{O}$ and $^*\text{OH}$) which may be somewhat too strong to proceed the oxygen evolution reaction efficiently. Therefore, to maintain the oxynitride perovskite photocatalysts for the long-term oxygen evolution, we must prevent their photo-oxidation and/or moderate a oxygen evolution intermediate binding. So far, the possible strategy is the introduction of photo-oxidation resistive materials and cocatalysts on their surfaces and there is still room to explore novel solutions. Further progress in the research regarding the above issues is awaited in the future for enabling their practical use for future hydrogen society.

Declaration of competing interest

The authors declare that they have no known competing financial interests or personal relationships that could have appeared to influence the work reported in this paper.

Acknowledgment

MH would like to thank the Alexander von Humboldt (AvH) Stiftung, Germany for the research award and The World Academy of Sciences (TWAS), Italy for the travel grant.

Notes:

[†]Crystal structure was drawn with VESTA 3 program (Momma and Izumi, 2011).

Appendix A. Supplementary data

Supplementary material related to this article can be found online at <https://doi.org/10.1016/j.egyr.2019.09.021>.

References

- Abeysinghe, D., Skrabalak, S.E., 2018. Toward shape-controlled metal oxynitride and nitride particles for solar energy applications. *ACS Energy Lett.* 3, 1331–1344.
- Bettine, K., Sahnoun, O., Sahnoun, M., Driz, M., 2017. Effect of anionic ordering on the electronic and optical properties of BaTaO_2N : TB-mBJ density functional calculation. *Chin. Phys. B* 26, 057101.
- Black, A.P., Suzuki, H., Higashi, M., Frontera, C., Ritter, C., De, C., Sundaresan, A., Abe, R., Fuertes, A., 2018. New rare earth hafnium oxynitride perovskites with photocatalytic activity in water oxidation and reduction. *Chem. Commun.* 54, 1525–1528.
- Boltersdorf, J., King, N., Maggard, P.A., 2015. Flux-mediated crystal growth of metal oxides: synthetic tunability of particle morphologies, sizes, and surface features for photocatalysis research. *Cryst. Eng. Commun.* 17, 2225–2241.
- Bugaris, D.E., zur Loye, H.-C., 2012. Materials discovery by flux crystal growth: Quaternary and higher order oxides. *Angew. Chem. Int. Ed.* 51, 3780–3811.
- Chen, Z., Dinh, H.N., Miller, E., 2013. Photoelectrochemical Water Splitting. Springer Briefs in Energy, New York, pp. 1–5.
- Cheviré, F., Tessier, F., Marchand, R., 2006. Optical properties of the perovskite solid solution $\text{LaTiO}_2\text{N-ATiO}_3$ ($A = \text{Sr, Ba}$). *Eur. J. Inorg. Chem.* 2006, 1223–1230.
- Cohen, I., Riess, I., 1994. Preparation of oxynitride thin films of $\text{BaNb(O}_y\text{N})_x$ and $\text{LaNb(O}_y\text{N}_2)_x$ using reactive sputtering from multiphase powder targets. *Mater. Sci. Eng. B* 25, 197–202.
- Cordes, N., Bräuniger, T., Schnick, W., 2018. Ammonothermal synthesis of $\text{EA MO}_2\text{N}$ ($\text{EA} = \text{Sr, Ba}; \text{M} = \text{Nb, Ta}$) perovskites and ^{14}N solid-state NMR spectroscopic investigations of AM(O,N)_3 ($A = \text{Ca, Sr, Ba, La}$). *Eur. J. Inorg. Chem.* 2018, 5019–5026.
- Dong, B., Qi, Y., Cui, J., Liu, B., Xiong, F., Jiang, X., Li, Z., Xiao, Y., Zhang, F., Li, C., 2017. Synthesis of BaTaO_2N oxynitride from Ba-rich oxide precursor for construction of visible-light-driven Z-scheme overall water splitting. *Dalton Trans.* 46, 10707–10713.
- Grigorescu, S., Bärhausen, B., Wang, L., Mazare, A., Yoo, J.E., Hahn, R., Schmuki, P., 2015. Tungsten doping of Ta_3N_5 -nanotubes for band gap narrowing and enhanced photoelectrochemical water splitting efficiency. *Electrochim. Commun.* 51, 85–88.
- Hafez, A.M., Zedan, A.F., AlQaradawi, S.Y., Salem, N.M., Allam, N.K., 2016. Computational study on oxynitride perovskites for CO_2 photoreduction. *Energy Convers. Manage.* 122, 207–214.
- Hibino, K., Yashima, M., Oshima, T., Fujii, K., Maeda, K., 2017. Structures, electron density and characterization of novel photocatalysts, $(\text{BaTaO}_2\text{N})_{1-x}(\text{SrWO}_2\text{N})_x$ solid solutions. *Dalton Trans.* 46, 14947–14956.
- Higashi, M., Abe, R., Takata, T., Domen, K., 2009. Photocatalytic overall water splitting under visible light using ATaO_2N ($A = \text{Ca, Sr, Ba}$) and WO_3 in a IO_3^-/I^- shuttle redox mediated system. *Chem. Mater.* 21, 1543–1549.
- Higashi, M., Domen, K., Abe, R., 2013. Fabrication of an efficient BaTaO_2N photoanode harvesting a wide range of visible light for water splitting. *J. Am. Chem. Soc.* 135, 10238–10241.
- Higashi, T., Shinohara, Y., Ohnishi, A., Liu, J., Ueda, K., Okamura, S., Hisatomi, T., Katayama, M., Nishiyama, H., Yamada, T., Minegishi, T., Domen, K., 2017. Sunlight-driven overall water splitting by the combination of surface-modified $\text{La}_5\text{Ti}_2\text{Cu}_{0.9}\text{Ag}_{0.1}\text{S}_5\text{O}_7$ and BaTaO_2N photoelectrodes. *Chem. Photo Chem.* 1, 167–172.
- Higashi, M., Yamanaka, Y., Tomita, O., Abe, R., 2015. Fabrication of cation-doped BaTaO_2N photoanodes for efficient photoelectrochemical water splitting under visible light irradiation. *APL Mater.* 3, 104418.
- Hisatomi, T., Katayama, C., Moriya, Y., Minegishi, T., Katayama, M., Nishiyama, H., Yamada, T., Domen, K., 2013. Photocatalytic oxygen evolution using BaNbO_2N modified with cobalt oxide under photoexcitation up to 740 nm. *Energy Environ. Sci.* 6, 3595–3599.
- Hisatomi, T., Katayama, C., Teramura, K., Takata, T., Moriya, Y., Minegishi, T., Katayama, M., Nishiyama, H., Yamada, T., Domen, K., 2014. The effects of preparation conditions for a BaNbO_2N photocatalyst on its physical properties. *Chem. Sus. Chem.* 7, 2016–2021.
- Hojamberdiev, M., Bekheet, M.F., Hart, J.N., Vequizo, J.J.M., Yamakata, A., Yubuta, K., Gurlo, A., Hasegawa, M., Domen, K., Teshima, K., 2017b. Elucidating the impact of A-site cation change on photocatalytic H_2 and O_2 evolution activities of perovskite-type LnTaON_2 ($\text{Ln} = \text{La and Pr}$). *Phys. Chem. Chem. Phys.* 19, 22210–22220.
- Hojamberdiev, M., Bekheet, M.F., Zahedi, E., Wagata, H., Vequizo, J.J.M., Yamakata, A., Yubuta, K., Gurlo, A., Domen, K., Teshima, K., 2016b. The contrasting effect of the Ta/Nb ratio in (111)-layered B-site deficient hexagonal perovskite $\text{Ba}_5\text{Nb}_{4-x}\text{Ta}_x\text{O}_{15}$ crystals on visible-light-induced photocatalytic water oxidation activity of their oxynitride derivatives. *Dalton Trans.* 45, 12559–12568.

- Hojamberdiev, M., Cai, Y., Vequizo, J.J.M., Mansoob Khan, M., Vargas, R., Yubuta, K., Yamakata, A., Teshima, K., Hasegawa, M., 2018. Binary flux-promoted formation of trigonal $ZnIn_2S_4$ layered crystals using ZnS-containing industrial waste and their photocatalytic performance for H_2 production. *Green Chem.* 20, 3845–3856.
- Hojamberdiev, M., Kawashima, K., Hisatomi, T., Katayama, M., Hasegawa, M., Domen, K., Teshima, K., 2019. Distinguishing the effects of altered morphology and size on visible-light-induced water oxidation activity and photoelectrochemical performance of $BaTaO_2N$ crystal structures. *Faraday Discuss.* 215, 227–241.
- Hojamberdiev, M., Kawashima, K., Kumar, M., Yamakata, A., Yubuta, K., Gurlo, A., Hasegawa, M., Domen, K., Teshima, K., 2017a. Engaging the flux-grown $La_{1-x}Sr_xFe_{1-y}Ti_yO_3$ crystals in visible-light-driven photocatalytic hydrogen generation. *Int. J. Hydrog. Energy* 42, 27024–27033.
- Hojamberdiev, M., Wagata, H., Yubuta, K., Kawashima, K., Vequizo, J.J.M., Yamakata, A., Oishi, S., Domen, K., Teshima, K., 2016a. KCl flux-induced growth of isometric crystals of cadmium-containing early transition-metal (Ti^{4+} , Nb^{5+} , and Ta^{5+}) oxides and nitridability to form their (oxy)nitride derivatives under an NH_3 atmosphere for water splitting application. *Appl. Catal. B* 182, 626–635.
- Hojamberdiev, M., Yamaguchi, A., Yubuta, K., Oishi, S., Teshima, K., 2015a. Fabrication of $La_2Ti_2O_7$ crystals using an alkali-metal molybdate flux growth method and their nitridability to form $LaTiO_2N$ crystals under a high-temperature NH_3 atmosphere. *Inorg. Chem.* 54, 3237–3244.
- Hojamberdiev, M., Yubuta, K., Vequizo, J.J.M., Yamakata, A., Oishi, S., Domen, K., Teshima, K., 2015b. NH_3 -assisted flux growth of cube-like $BaTaO_2N$ submicron crystals in a completely ionized nonaqueous high-temperature solution and their water splitting activity. *Cryst. Growth Des.* 15, 4663–4671.
- Hojamberdiev, M., Zahedi, E., Nurlaela, E., Kawashima, K., Yubuta, K., Nakayama, M., Wagata, H., Minegishi, T., Domen, K., Teshima, K., 2016c. The cross-substitution effect of tantalum on the visible-light-driven water oxidation activity of $BaNbO_2N$ crystals grown directly by an NH_3 -assisted flux method. *J. Mater. Chem. A* 4, 12807–12817.
- Kasahara, A., Nukumizu, K., Hitoki, G., Takata, T., Kondo, J.N., Hara, M., Kobayashi, H., Domen, K., 2002. Photoreactions on $LaTiO_2N$ under visible light irradiation. *J. Phys. Chem. A* 106, 6750–6753.
- Kasahara, A., Nukumizu, K., Takata, T., Kondo, J.N., Hara, M., Kobayashi, H., Domen, K., 2003. $LaTiO_2N$ as a visible-light (≤ 600 nm)-driven photocatalyst (2). *J. Phys. Chem. B* 107, 791–797.
- Kawashima, K., Hojamberdiev, M., Mabayoje, O., Wygant, B.R., Yubuta, K., Mullins, C.B., Domen, K., Teshima, K., 2017b. NH_3 -assisted chloride flux-coating method for direct fabrication of visible-light-responsive $SrNbO_2N$ crystal layers. *Cryst. Eng. Commun.* 19, 5532–5541.
- Kawashima, K., Hojamberdiev, M., Stabler, C., Vrankovic, D., Yubuta, K., Riedel, R., Domen, K., Teshima, K., 2017a. Perovskite $Sr_{1-x}Ba_xW_{1-y}Ta_y(O,N)_3$: synthesis by thermal ammonolysis and photocatalytic oxygen evolution under visible light. *Mater. Renew. Sustain. Energy* 6 (2), 10.
- Kawashima, K., Hojamberdiev, M., Wagata, H., Nakayama, M., Yubuta, K., Oishi, S., Domen, K., Teshima, K., 2016a. Amount of tungsten dopant influencing the photocatalytic water oxidation activity of $LaTiO_2N$ crystals grown directly by an NH_3 -assisted flux method. *Catal. Sci. Technol.* 6, 5389–5396.
- Kawashima, K., Hojamberdiev, M., Wagata, H., Yubuta, K., Oishi, S., Teshima, K., 2014. Chloride flux growth of $La_2Ti_2O_7$ crystals and nontopotactic solid-state transformation to $LaTiO_2N$ crystals by nitridation using NH_3 . *Cryst. Growth Des.* 15, 333–339.
- Kawashima, K., Hojamberdiev, M., Wagata, H., Yubuta, K., Vequizo, J.J.M., Yamakata, A., Oishi, S., Domen, K., Teshima, K., 2015. NH_3 -assisted flux-mediated direct growth of $LaTiO_2N$ crystallites for visible-light-induced water splitting. *J. Phys. Chem. C* 119, 15896–15904.
- Kawashima, K., Hojamberdiev, M., Wagata, H., Zahedi, E., Yubuta, K., Domen, K., Teshima, K., 2016b. Two-step synthesis and visible-light-driven photocatalytic water oxidation activity of $AW(O,N)_3$ ($A = Sr, La, Pr, Nd$ and Eu) perovskites. *J. Catal.* 344, 29–37.
- Kawashima, K., Hojamberdiev, M., Yubuta, K., Domen, K., Teshima, K., 2018a. Synthesis and visible-light-induced sacrificial photocatalytic water oxidation of quininary oxynitride $BaNb_{0.5}Ta_{0.5}O_2N$ crystals. *J. Energy Chem.* 27, 1415–1421.
- Kawashima, K., Kim, J.-H., Cheng, I., Yubuta, K., Shin, K., Liu, Y., Lin, J., Henkelman, G., Mullins, C.B., 2018b. Chloride flux growth of idiomorphic AWO_4 ($A = Sr, Ba$) single microcrystals. *Cryst. Growth Des.* 18, 5301–5310.
- Kawashima, K., Liu, Y., Kim, J.H., Wygant, B.R., Cheng, I., Celio, H., Mabayoje, O., Lin, J., Mullins, C.B., 2019. Infrared light-driven $LaW(O,N)_3$ OER photoelectrocatalysts from chloride flux-grown $La_4W_3O_{15}$ templating precursors. *ACS Appl. Energy Mater.* 2, 913–922.
- Kim, Y.-I., Woodward, P.M., Baba-Kishi, K.Z., Tai, C.W., 2004. Characterization of the structural, optical, and dielectric properties of oxynitride perovskites AMO_2N ($A = Ba, Sr, Ca; M = Ta, Nb$). *Chem. Mater.* 16, 1267–1276.
- Kodera, M., Katayama, M., Hisatomi, T., Minegishi, T., Domen, K., 2016. Effects of flux treatment on morphology of single-crystalline $BaNbO_2N$ particles. *Cryst. Eng. Commun.* 18, 3186–3190.
- Kubo, A., Giorgi, G., Yamashita, K., 2017. $MgTaO_2N$ photocatalysts: Perovskite versus ilmenite structure. A theoretical investigation. *J. Phys. Chem. C* 121, 27813–27821.
- Kudo, A., Miseki, Y., 2009. Heterogeneous photocatalyst materials for water splitting. *Chem. Soc. Rev.* 38, 253–278.
- Lee, J.S., 2005. Photocatalytic water splitting under visible light with particulate semiconductor catalysts. *Catal. Surv. Asia* 9, 217–227.
- Liu, J., Liu, Y., Liu, N., Han, Y., Zhang, X., Huang, H., Lifshitz, Y., Lee, S.T., Zhong, J., Kang, Z., 2015. Metal-free efficient photocatalyst for stable visible water splitting via a two-electron pathway. *Science* 347, 970–974.
- Logvinovich, D., Börger, A., Döbeli, M., Ebbinghaus, S.G., Reller, A., Weidenkaff, A., 2007. Synthesis and physical chemical properties of Ca-substituted $LaTiO_2N$. *Prog. Solid State Chem.* 35, 281–290.
- Maeda, K., 2011. Photocatalytic water splitting using semiconductor particles: history and recent developments. *J. Photochem. Photobiol. C: Photochem. Rev.* 12, 237–268.
- Maeda, K., Domen, K., 2007. New non-oxide photocatalysts designed for overall water splitting under visible light. *J. Phys. Chem. C* 111, 7851–7861.
- Maeda, K., Domen, K., 2010. Photocatalytic water splitting: recent progress and future challenges. *J. Phys. Chem. Lett.* 1, 2655–2661.
- Maeda, K., Domen, K., 2011. Oxynitride materials for solar water splitting. *MRS Bull.* 36, 25–31.
- Maeda, K., Domen, K., 2012. Water oxidation using a particulate $BaZrO_3$ – $BaTaO_2N$ solid-solution photocatalyst that operates under a wide range of visible light. *Angew. Chem. Int. Ed.* 51, 9865–9869.
- Maeda, K., Lu, D., Domen, K., 2013a. Oxidation of water under visible-light irradiation over modified $BaTaO_2N$ photocatalysts promoted by tungsten species. *Angew. Chem.* 125, 6616–6619.
- Maeda, K., Lu, D., Domen, K., 2013b. Oxidation of water under visible-light irradiation over modified $BaTaO_2N$ photocatalysts promoted by tungsten species. *Angew. Chem. Int. Ed.* 52, 6488–6491.
- Maeda, K., Teramura, K., Lu, D., Takata, T., Saito, N., Inoue, Y., Domen, K., 2006. Photocatalyst releasing hydrogen from water. *Nature* 440, 295.
- Maegli, A.E., Hisatomi, T., Otal, E.H., Yoon, S., Pokrant, S., Grätzel, M., Weidenkaff, A., 2012a. Structural and photocatalytic properties of perovskite-type $(La,Ca)Ti(O,N)_3$ prepared from A-site deficient precursors. *J. Mater. Chem.* 22, 17906–17913.
- Maegli, A.E., Otal, E.H., Hisatomi, T., Yoon, S., Leroy, C.M., Schäuble, N., Lu, Y., Grätzel, M., Weidenkaff, A., 2012b. Perovskite-type $LaTiO_2N$ oxynitrides for solar water splitting: Influence of the synthesis conditions. *Energy Procedia* 22, 61–66.
- Maegli, A.E., Pokrant, S., Hisatomi, T., Trottmann, M., Domen, K., Weidenkaff, A., 2013. Enhancement of photocatalytic water oxidation by the morphological control of $LaTiO_2N$ and cobalt oxide catalysts. *J. Phys. Chem. C* 118, 16344–16351.
- Marchand, R., Pors, F., Laurent, Y., Regreny, O., Lostec, J., Haussonne, J.M., 1986. Perovskites oxynitrurees utilisees en tant que materiaux dielectriques. *J. Phys. Colloq.* 47, C1–901–C1–905.
- Momma, K., Izumi, F., 2011. VESTA 3 for three-dimensional visualization of crystal, volumetric and morphology data. *J. Appl. Crystallogr.* 44, 1272–1276.
- Montoya, J.H., Garcia-Mota, M., Nørskov, J.K., Vojvodic, A., 2015. Theoretical evaluation of the surface electrochemistry of perovskites with promising photon absorption properties for solar water splitting. *Phys. Chem. Chem. Phys.* 17, 2634–2640.
- Moon, K.-H., Kim, J.-M., Sohn, Y., Cho, D.W., Kim, Y.-I., Avdeev, M., 2016. Crystal structures and color properties of new complex perovskite oxynitrides $AMg_{0.2}Ta_{0.8}O_{2.6}N_{0.4}$ ($A = Sr, Ba$). *Dalton Trans.* 45, 5614–5621.
- Moriga, T., Ikeuchi, K., Mashima, R., Aoki, D., Murai, K.I., 2007. Influence of cation nonstoichiometry on the optical properties of the perovskite-type oxynitride $LaTiO_2N$. *J. Ceram. Soc. Japan* 115, 637–639.
- Moriya, Y., Takata, T., Domen, K., 2013. Recent progress in the development of (oxy)nitride photocatalysts for water splitting under visible-light irradiation. *Coord. Chem. Rev.* 257, 1957–1969.
- Niu, W.-B., Sun, S.-K., Guo, W.-M., Chen, S.-L., Lv, M., Lin, H.-T., Wang, C.-Y., 2018. Synthesis of perovskite $BaTaO_2N$ and $SrNbO_2N$ using TaN/NbN as the nitrogen source. *Ceram. Int.* 44, 23324–23328.
- Oishi, S., Tate, I., Hirano, S., Naka, S., 1984. Choice of fluxes for the crystal growth of oxides from high-temperature solutions. *Nippon Kagaku Kaishi* 5, 685–690, (in Japanese).
- Okamoto, H., Kodera, M., Hisatomi, T., Katayama, M., Minegishi, T., Domen, K., 2019. Effects of annealing conditions on the oxygen evolution activity of a $BaTaO_2N$ photocatalyst loaded with cobalt species. *Catal. Today* <http://dx.doi.org/10.1016/j.cattod.2018.12.048>, (in press).
- Osterloh, F.E., 2013. Inorganic nanostructures for photoelectrochemical and photocatalytic water splitting. *Chem. Soc. Rev.* 42, 2294–2320.
- Ouhbi, H., Aschauer, U., 2019. Nitrogen loss and oxygen evolution reaction activity of perovskite oxynitrides. *ACS Materials Lett.* 1, 52–57.

- Pors, F., Marchand, R., Laurent, Y., Bacher, P., Roult, G., 1988. Etude structurale des perovskites oxyazotees BaTaO₂N et BaNbO₂N: Structural study of BaTaO₂N and BaNbO₂N oxynitrided perovskites. Mater. Res. Bull. 23, 1447–1450, (in French).
- Seo, J., Hisatomi, T., Nakabayashi, M., Shibata, N., Minegishi, T., Katayama, M., Domen, K., 2018. Efficient solar-driven water oxidation over perovskite-type BaNbO₂N photoanodes absorbing visible light up to 740 nm. Adv. Energy Mater. 8, 1800094.
- Seo, J., Moriya, Y., Kodera, M., Hisatomi, T., Minegishi, T., Katayama, M., Domen, K., 2016. Photoelectrochemical water splitting on particulate ANbO₂N (A = Ba, Sr) photoanodes prepared from perovskite-type ANbO₃. Chem. Mater. 28, 6869–6876.
- Seo, J., Nakabayashi, M., Hisatomi, T., Shibata, N., Minegishi, T., Katayama, M., Domen, K., 2019. The effects of annealing barium niobium oxynitride in argon on photoelectrochemical water oxidation activity. J. Mater. Chem. A 7, 493–502.
- Setsuda, Y., Maruyama, Y., Izawa, C., Watanabe, T., 2017. Low-temperature synthesis of BaTaO₂N via the flux method using NaNH₂. Chem. Lett. 46, 987–989.
- Siritanarakul, B., Maeda, K., Hisatomi, T., Domen, K., 2011. Synthesis and photocatalytic activity of perovskite niobium oxynitrides with wide visible-light absorption bands. Chem. Sus. Chem. 4, 74–78.
- Strukova, G.K., Kedrov, V.V., Zverev, V.N., Khasanov, S.S., Ovchinnikov, I.M., Batov, I.E., Gasparov, V.A., 1997. On the synthesis and the electric and magnetic properties of superconducting barium-niobium-oxide compounds. Physica C 291, 207–212.
- Sun, S.-K., Masubuchi, Y., Motohashi, T., Kikkawa, S., 2015. Direct synthesis of nearly single-phase BaTaO₂N and CaTaO₂N powders. J. Eur. Ceram. Soc. 35, 3289–3294.
- Teshima, K., Hara, Y., Yubuta, K., Oishi, S., Domen, K., Hojamberdiev, M., 2017. Application of flux method to the fabrication of Ba₅Ta₄O₁₅, Sr₅Ta₄O₁₅, Sr₂Ta₂O₇, and BaTaO₂N polycrystalline films on Ta substrates. Cryst. Growth Des. 17, 1583–1588.
- Tessier, F., 2018. Determining the nitrogen content in (oxy)nitride materials. Materials 11 (8), 1331.
- Tessier, F., Le Gendre, L., Cheviré, F., Marchand, R., Navrotsky, A., 2005. Thermochemistry of a new class of materials containing dinitrogen pairs in an oxide matrix. Chem. Mater. 17, 3570–3574.
- Tessier, F., Marchand, R., 2003. Ternary and higher order rare-earth nitride materials: synthesis and characterization of ionic-covalent oxynitride powders. J. Solid State Chem. 171, 143–151.
- Ueda, K., Minegishi, T., Clune, J., Nakabayashi, M., Hisatomi, T., Nishiyama, H., Katayama, M., Shibata, N., Kubota, J., Yamada, T., Domen, K., 2015. Photoelectrochemical oxidation of water using BaTaO₂N photoanodes prepared by particle transfer method. J. Am. Chem. Soc. 137, 2227–2230.
- Vequizo, J.J.M., Hojamberdiev, M., Teshima, K., Yamakata, A., 2018. Role of CoO_x Cocatalyst on Ta₃N₅ photocatalysts studied by transient visible to mid-infrared absorption spectroscopy. J. Photochem. Photobiol. A 358, 315–319.
- Wagata, H., Sakakibara, K., Kawashima, K., Hojamberdiev, M., Yubuta, K., Teshima, K., 2019. Alkali metal chloride flux growth of ilmenite-type ZnTiO₃ and subsequent nitrogen doping for visible-light-driven water oxidation catalysis. ACS Appl. Energy Mater. <http://dx.doi.org/10.1021/acsae.9b00815>, (in press).
- Wagata, H., Zettsu, N., Yamaguchi, A., Nishikiori, H., Yubuta, K., Oishi, S., Teshima, K., 2014. Chloride flux growth of La₂Ti₂O₇ crystals and subsequent nitridation to form LaTiO₂N crystals. Cryst. Growth Des. 15, 124–128.
- Wang, C., Hisatomi, T., Minegishi, T., Wang, Q., Zhong, M., Katayama, M., Kubota, J., Domen, K., 2016. Synthesis of nanostructured BaTaO₂N thin films as photoanodes for solar water splitting. J. Phys. Chem. C 120, 15758–15764.
- Wei, S., Jin, S., Pan, G., Li, Z., Liu, G., Xu, X., 2019. Triggering efficient photocatalytic water oxidation reactions over BaNbO₂N by incorporating Ca at B site. J. Am. Ceram. Soc. 102, 6194–6201.
- Wei, S., Zhang, G., Xu, X., 2018. Activating BaTaO₂N by Ca modifications and cobalt oxide for visible light photocatalytic water oxidation reactions. Appl. Catal. B 237, 373–381.
- Wu, F., Liu, G., Xu, X., 2017. Efficient photocatalytic oxygen production over Ca-modified LaTiO₂N. J. Catal. 346, 10–20.
- Xiong, F.Q., Wan, L., Li, Y., Thomas, T., DiSalvo, F.J., Yang, M., 2017. Crucial role of donor density in the performance of oxynitride perovskite LaTiO₂N for photocatalytic water oxidation. Chem. Sus. Chem. 10, 930–937.
- Yamada, T., Murata, Y., Suzuki, S., Wagata, H., Oishi, S., Teshima, K., 2018. Template-assisted size control of polycrystalline BaNbO₂N particles and effects of their characteristics on photocatalytic water oxidation performances. J. Phys. Chem. C 122, 8037–8044.
- Yashima, M., Saito, M., Nakano, H., Takata, T., Ogisu, K., Domen, K., 2010. *Imma* perovskite-type oxynitride LaTiO₂N: structure and electron density. Chem. Commun. 46, 4704–4706.
- Zhang, F., Yamakata, A., Maeda, K., Moriya, Y., Takata, T., Kubota, J., Teshima, K., Oishi, S., Domen, K., 2012. Cobalt-modified porous single-crystalline LaTiO₂N for highly efficient water oxidation under visible light. J. Am. Chem. Soc. 134, 8348–8351.
- Zou, Z., Ye, J., Sayama, K., Arakawa, H., 2001. Direct splitting of water under visible light irradiation with an oxide semiconductor photocatalyst. Nature 414, 625–627.